Bulletin of Engineering Geology and the Environment (2019) 78:3449–3464
https://doi.org/10.1007/s10064-018-1336-0

ORIGINAL PAPER

Deformation failure characteristics of coal–rock combined body under uniaxial compression: experimental and numerical investigations

Yulong Chen [1,2] · Jianping Zuo [1,3] · Dejun Liu [3] · Zhenbo Wang [3]

Received: 28 March 2018 / Accepted: 23 June 2018 / Published online: 10 July 2018

Abstract

The deformation and failure behaviour of coal–rock combined body under uniaxial compression were investigated experimentally and numerically. The mechanical parameters, including the uniaxial compressive strength (UCS), elastic modulus and full-scale stress–strain curves, were obtained. A detailed analysis of the evolution of the internal cracks based on X-ray computed tomography (CT) observations and acoustic emission (AE) locations is presented. The experimental results show that the mechanical properties and deformation failure characteristics of the coal–rock combined body were governed mainly by the coal. The UCS and elastic modulus of the coal–rock combined body were slightly larger than those of the coal and most of the cracks occurring in the coal were a result of the uniaxial compression. Furthermore, a numerical simulation was conducted to validate the experimental evidence. Finally, based on this understanding, a constitutive relationship was proposed using the natural strain described in Hooke's law for accurate modelling of the deformation of the coal–rock body. A good agreement was obtained between the numerical results and experimental data during the pre-peak regime.

Keywords Coal–rock combined body · Uniaxial compression · Deformation failure · Constitutive relationship

Introduction

With a continued focus on energy-related problems, China has focused a significant amount of attention on deep coal mining. However, as the mining depth of Chinese coal mines has increased, especially large-scale high-caving mining and thick coal seam mining, many mine disasters have occurred, although the number of deaths has decreased in recent years. Many coal pillars, such as section pillars, pillar mining and pillars that are used to protect faults, for strip mining and for rooms, are kept intact to achieve a safe and efficient mining operation at the working face (Wang et al. 2013; Ghasemi et al. 2014). Therefore, a distinctive composite model of rock masses composed of soft coal and relatively hard rock is formed. In this regard, the physical and mechanical behaviours of coal and rock are very important to evaluate the stability of the rock strata and coal pillar around the working face. Both laboratory tests and field observations have indicated that underground excavation and mining caused marked damage to both coal and rock bodies (Kwinta 2012; Konicek et al. 2013; Zhu et al. 2014; Cao et al. 2015; Gao et al. 2015; Meng et al. 2016). A large-scale physical model has been created to simulate a massive roof collapse during longwall coal retreat mining (Kang et al. 2018). In addition, numerical methods have been widely applied to investigate coal/rock failures and outbursts in coal mines (Li et al. 2011; Gao et al. 2014, 2015). This is an inevitable consequence of stress relief that accompanies any excavation and mining activity (Qian 2004; Xie et al. 2012b).

Excavation disturbed zones and excavation damaged zones result from the excavation of underground openings (Tsang et al. 2005; Wang et al. 2017a). In coal mining processes, both coal and rock are excavated in a working panel or roadway. The applied stress usually increases due to the coal–rock interaction in front of the coal working face. This process may crush the coal and possibly trigger coal and gas outbursts (Xie et al. 2012a; Yang et al. 2012, 2018). Figure 1 shows the schematic of an area of coal and rock excavation. Most

✉ Jianping Zuo
zjp@cumtb.edu.cn

[1] State Key Laboratory of Coal Resources and Safe Mining, China University of Mining and Technology, Beijing 100083, China

[2] State Key Laboratory of Hydroscience and Engineering, Tsinghua University, Beijing 100084, China

[3] School of Mechanics and Civil Engineering, China University of Mining and Technology, Beijing 100083, China

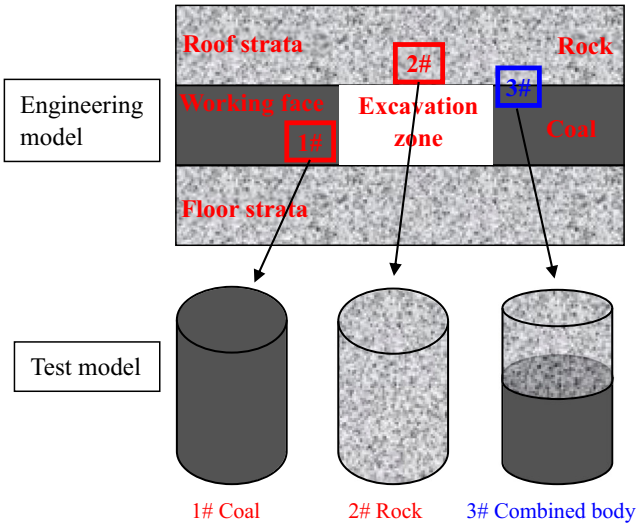

Fig. 1 A schematic diagram of an engineering mining activity and test models in three typical failure zones

research studies have focused on the failure of coal or rock bodies, such as those in position #1 and position #2 (Paterson and Wong 2005). However, few experimental studies have focused on the failure of bodies in position #3. In fact, there is a zone of concentrated stress near the area of position #3. Field observations of a large number of disasters have clearly indicated that the failures were not caused by a single rock mass or coal seam but by the structural failure of the coal–rock combined body. In other words, these disasters are induced not only by the local material failure but also by the structural failure of the coal–rock combination (Zhao et al. 2015). Based on some actual mining activities, such as continued excavation and blasting, the combined bodies of coal and rock are normally subject to different stress states and may suddenly fail.

A limited number of studies have been published on the mechanical behaviour of coal–rock combined bodies. Petukhov and Linkov (1979) were the first to determine the stability of a two-body system composed of the roof, floor and coal. Wang et al. (2014) carried out a double-shear frictional test of a composite sandstone–coal sample under biaxial loading and discussed the space–time evolution of the displacement field, as well as the acoustic emission (AE) characteristics during sliding. Zhao et al. (2015) investigated the failure characteristics and compression–shear strength criterion of a coal–rock combination model. Liu et al. (2015) studied the effect of the rock strength on the failure mode and mechanical behaviour of composite bodies, and drew the conclusion that the peak strength of the combined bodies decreased with increasing rock strength. Wang et al. (2017b) studied the mechanical behaviour and seepage characteristics of gas-bearing coals and coal–rock combined bodies under triaxial conditions. Although previous studies have yielded many facts on the failure mechanism and mechanical behaviour of coal–rock combined bodies, more research work is needed to illuminate the dark corners of the comprehensive studies of the mechanical and stability properties of coal–rock combined bodies.

In this study, we attempt to improve our knowledge of the deformation failure characteristics of coal–rock combined bodies with the expectation to supply some basic information support for mining engineering. To this end, uniaxial compressive tests were conducted on the coal–rock combined body to obtain the uniaxial compressive strength (UCS), elastic modulus and complete stress–strain curves. We also analysed the evolution of the damage of the specimens using the spatial and temporal distribution of the AE counts. In addition, X-ray computed tomography (CT) was performed on the specimens after the uniaxial compression failure to analyse the internal damage characteristics. In addition, a numerical simulation of the experimental tests of the uniaxial compression was conducted to interpret the failure mechanism and patterns of the coal–rock combined body. Finally, a constitutive model was formulated based on the experimental data to describe the mechanical behaviour of the coal–rock combined body.

Experimental materials and methods

Specimen preparation

The surrounding rock, which was sandstone, and the coal samples were obtained from the working face #2071 of the Qianjiaying colliery in Hebei Province, China, at a buried depth of about 850 m. Large intact rock and coal blocks were drilled from the working face. The rock and coal blocks were directly transported to the laboratory and individually shaped into cylindrical specimens of Φ 35 mm × L 35 mm. The ends were polished to a parallelism of 2/100. The combined coal–rock body was composed of a coal and a rock sample with the same dimensions (Φ35 mm × L 35 mm). Therefore, the total dimension of the combined body was Φ 35 mm × L 70 mm and had a length to diameter ratio of 2.0. To reduce the factors influencing the failure of the combined specimens, the coal part and rock part were in direct contact with each other, without the use of any superglue at the interface (Zuo et al. 2016).

Two combination patterns of the coal and rock were prepared. The coal was on the top or bottom of the rock to simulate the actual conditions of the floor or roof, respectively, in the mining operation. The coal was affixed to the top or bottom of the rock using a piece of Scotch tape in the middle of the combined body and was in direct contact with the rock at the top or bottom. The images of the coal–rock combined body specimens are shown in Fig. 2. Ultrasonic wave analysis was used to determine the internal microstructure of the combined body specimens. The sample details are presented in

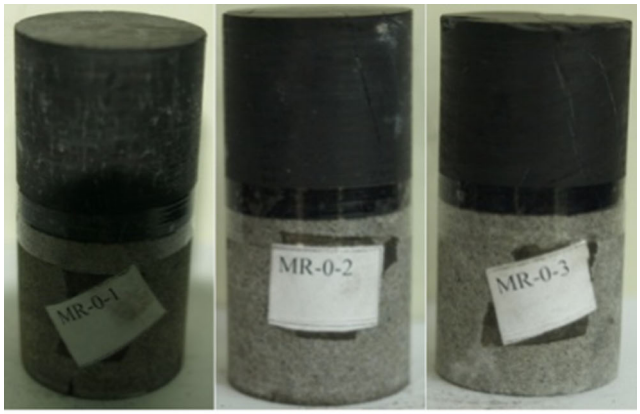

(a) MR

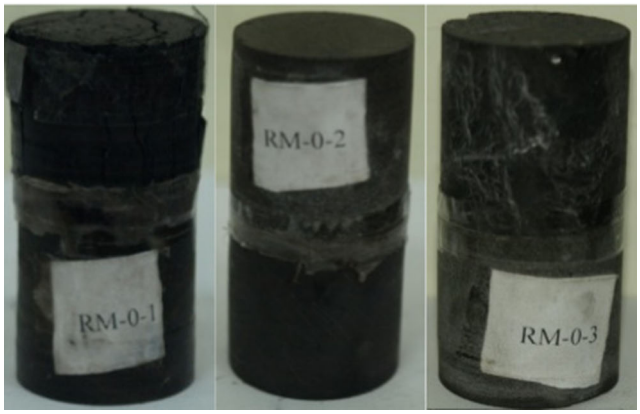

(b) RM

Fig. 2 Photographs of the coal–rock combined body samples

Table 1. The nomenclature of the test designations is provided in the first column of Table 1 in the form of "MR (or RM)-0-1~3", indicating the combination patterns (MR: coal above rock; RM: coal below rock), the unconfined stress and the sample number, respectively.

An X-ray diffraction test was performed to determine the mineral composition of the rock and coal (Fig. 3). The mineralogical constitution of the rock mainly included quartz, clay and small amounts of siderite and dolomite. The coal consisted of non-crystal material, clay and a small percentage of siderite, dolomite and calcite. The lithology has a significant effect on the mechanical characteristics due to the differences in the mineral constituents and structures (Zhang et al. 2015, 2017). The differences in the mineral composition and microstructure between the rock and the coal provide a reference and micro-mechanical foundation for the analysis of the deformation failure characteristics of the coal–rock combined body presented later in this paper.

Testing equipment

The MTS 815 testing system was used to test the samples. The maximum axial load capacity is 4600 kN. The horizontal and axial ranges of the extensometer are ± 4 mm and − 2.5 to + 12.5 mm, respectively. Since the failure strengths of both the coal and rock are very small in relation to the measurement range of the test apparatus, the machine can be regarded as a rigid test machine, which meets the requirement of the International Society for Rock Mechanics (ISRM) (Ulusay and Hudson 2007). The AE output was recorded by a PCI-2 AE 3D measuring system made by Physical Acoustics Corp. (PAC); six AE sensors were attached to the specimens to obtain the spatial distribution of the AE events and the sampling rate was 40 m/s. The experimental setup for a sample is illustrated in Fig. 4.

Table 1 Physical and mechanical properties of coal–rock combined body specimens under uniaxial compression

Sample no.	Pattern	Length (mm)	Diameter (mm)	Wave velocity (m/s)	Elastic modulus (GPa)	UCS (MPa)	Strain at peak stress (‰)		
							ε_1	ε_r	ε_v
MR-0-1	Coal	35.38	34.56	2656.18	6.33	28.39	7.89	− 10.52	− 13.14
	Rock	34.43	34.94						
MR-0-2	Coal	35.86	34.77	2360.66	5.41	25.44	8.20	− 6.35	− 4.51
	Rock	34.49	34.89						
MR-0-3	Coal	34.95	34.81	2313.25	5.22	21.02	7.29	− 9.54	− 11.78
	Rock	35.00	34.43						
RM-0-1	Rock	34.51	34.39	2451.01	7.45	27.31	5.81	− 10.45	− 15.10
	Coal	33.60	34.67						
RM-0-2	Rock	35.43	34.49	2293.25	6.61	23.58	6.01	− 4.40	− 2.78
	Coal	35.05	34.65						
RM-0-3	Rock	34.01	34.90	1611.18	5.79	19.76	4.56	− 3.77	− 2.97
	Coal	35.15	34.29						

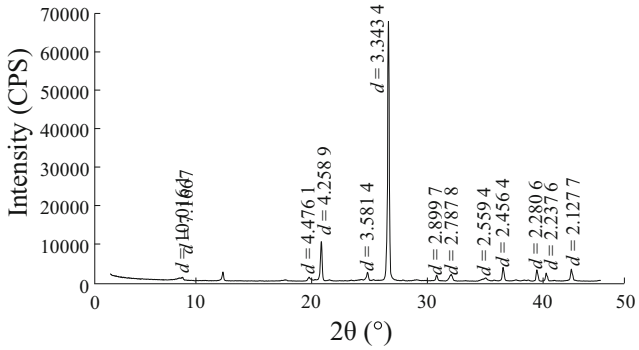

(a) Rock

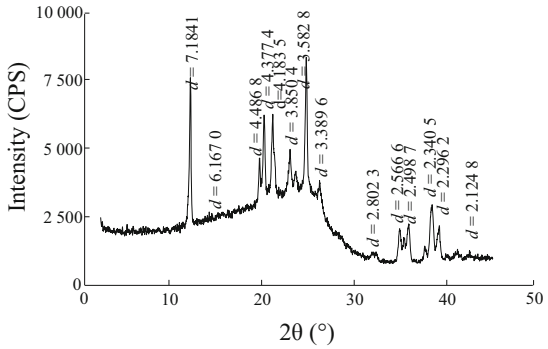

(b) Coal

Fig. 3 X-ray diffraction patterns of the rock (**a**) and coal (**b**) samples

The X-ray CT scanning of the specimens was carried out using a Nanotom 160 high-resolution micro-CT at a spatial resolution of 30 μm to explore the internal damage in the post-compression specimens. Each sample was scanned before and after the tests. In the present research, 21 horizontal cross-sections and one vertical cross-section were scanned for every specimen.

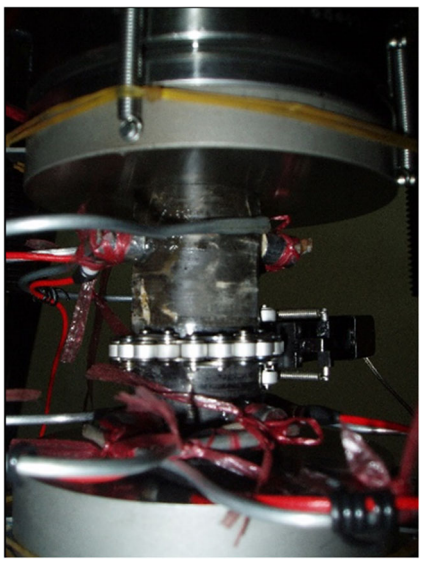

Fig. 4 The uniaxial compression test setup

Testing procedure

Full-regime uniaxial compression tests of the samples were conducted with real-time AE monitoring and positioning. An axial displacement rate of 0.06 mm/min was applied until the residual stress stage. Subsequently, the axial displacement rate was increased to 0.1 mm/min.

Experimental results

Stress–strain relations

The uniaxial compression tests were performed on the three coal–rock combined body specimens for each combination pattern and the physical and mechanical properties are listed in Table 1. The stress–strain curves of the coal–rock combined body are presented in Fig. 5, where ε_1, ε_r and ε_v represent the axial strain, radial strain and volumetric strain, respectively. ε_v is the sum of the axial strain and twice the radial strain, i.e. $\varepsilon_v = \varepsilon_1 + 2\varepsilon_r$. It should be noted that the positive and negative values of the strain refer to the compressive and dilatation deformations, respectively. A similar behaviour was observed for the six specimens. As for most geomaterials, the coal–rock combined body exhibits a pressure-dependent behaviour. Generally, the stress–strain curves of the coal–rock combined body underwent six stages: compaction stage, linear elastic deformation stage, inelastic deformation stage, strain-hardening stage, post-peak softening stage and residual strength stage, as shown in Fig. 6. The compaction stage under uniaxial compression was very obvious, showing an inelastic, concave-upward shape, which is due to the closure of the existing microcracks and interface between the coal and rock. The subsequent linear elastic deformation stage dominated the linear portions of the stress–strain curves; during this stage, the matrix deformed and the material exhibited intact geomaterial behaviour characterised by a constant stiffness. This was followed by an inelastic deformation stage, during which the curve lost its linearity and a significant increase in the strain occurred as the microfractures began to propagate in a stable manner. With the increase in the stress, the specimens entered a strain-hardening stage, during which the crack initiation and propagation led to a strain increase in an unstable manner up to the peak stress, where an asymptotic failure state was observed. Once the peak stress was reached, there was a post-peak softening stage characterised by an obvious brittle drop in the stress, during which the macrocracks coalesced but the rock remained intact, even though its internal structure was highly disrupted. Finally, the specimens entered the residual strength stage, during which the specimen was divided to form a series of blocks with a constant drop in the residual strength.

During the loading process, the volume change in the specimens mainly resulted from the propagation of microcracks

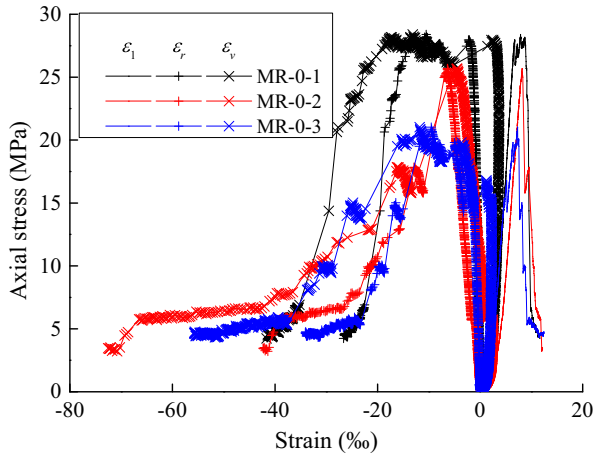

(a) MR

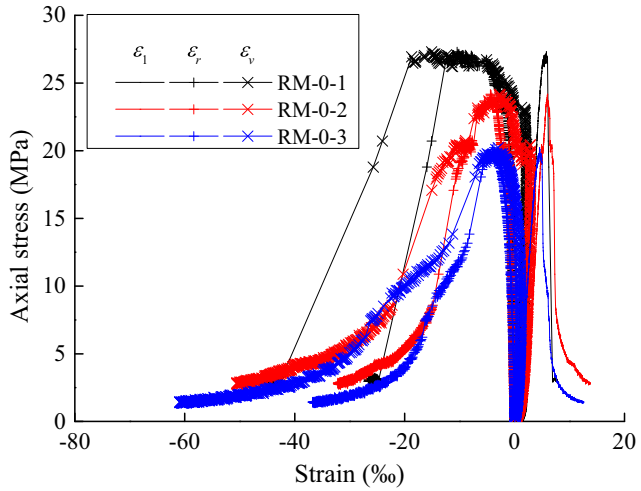

(b) RM

Fig. 5 Stress–strain curves of the coal–rock combined body under uniaxial compression

and the volumetric strain was divided into two stages. At the initial low stress, primary microfissures, as well as the interface between the coal and rock, were closed; the radial strain was small, leading to volume compression without generating new damage. With the increase in the stress, the cracks propagated and rock damage began to develop. As a result, the radial expansion gradually became predominant and volumetric dilatancy occurred. When the specimen failed, the sample volume dilated rapidly until a large strain occurred due to the coalescence of the cracks.

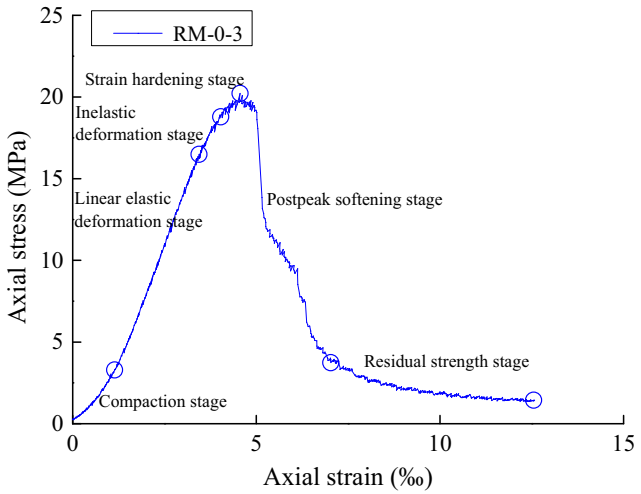

Fig. 6 A typical stress–strain curve of the coal–rock combined body

UCS and elastic modulus

The UCS refers to the maximum axial stress in a stress–strain curve under uniaxial compression and the elastic modulus is the slope of the approximately straight-line portion of the curve prior to the peak stress. Table 1 lists the values of the UCS and elastic modulus of the coal–rock combination specimens in this study. Based on the data listed in Table 1, Fig. 7 shows the average UCS and elastic modulus of the coal–rock combination, rock and coal bodies.

The average UCS was 24.95 MPa for the MR specimens and 23.55 MPa for the RM specimens, and the average elastic modulus was 5.65 GPa for the MR specimens and 6.62 GPa

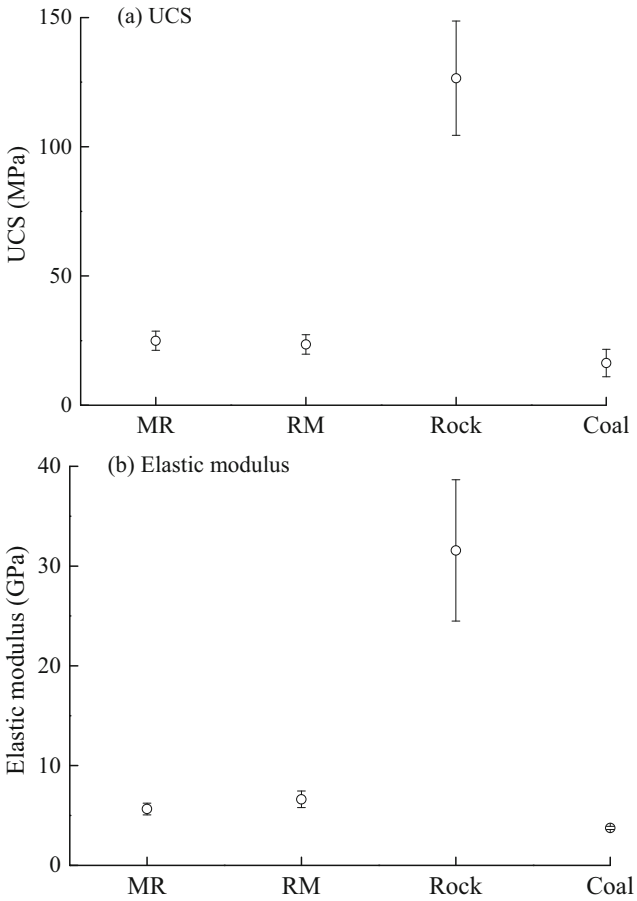

Fig. 7 Average uniaxial compressive strength (UCS) and elastic modulus of coal–rock combination, rock and coal bodies. The error bars range from the minimum to the maximum measured values

for the RM specimens. It can be seen that the values of the UCS and elastic modulus were similar for the two types of combination patterns, indicating that the combination pattern did not affect the UCS and elastic modulus of the coal–rock combined body.

The UCS and elastic modulus for rock and coal bodies were also obtained for comparison purposes from published data (Zuo et al. 2011a, b). The average UCS was 126.52 MPa and 16.32 MPa and the average elastic modulus was 31.57 GPa and 3.75 GPa for rock and coal, respectively.

The average UCS and elastic modulus values of the two types of coal–rock combined bodies were between the values of the rock and coal and were around 80% lower than those of the rock body and 44–76% higher than those of the coal body, indicating that the mechanical properties of the coal–rock combined body were governed by the coal, which is the weakest part.

The wave velocity, elastic modulus and UCS of the coal–rock combined bodies exhibited slight differences, which may be attributed to pre-existing microcracks in the coal and rock. The X-ray CT scanning was not performed prior to the tests; therefore, pre-existing cracks were not identified. In this study, we focus on a qualitative analysis of the deformation failure characteristics of the coal–rock combined body. The specimens of the coal–rock combined bodies showed similar deformation failure characteristics, although the distributions of the pre-existing cracks may have differed for the bodies. The effect of the pre-existing microcracks on the discreteness of the wave velocity, elastic modulus and UCS did not impact the qualitative experimental results on the coal–rock combined bodies.

Fracture mode

Figure 8 illustrates the fracture characteristics of the coal–rock combination specimens under uniaxial compression. The results show that the cracks mainly occurred in the coal and there were almost no visible cracks in the rock portion because the applied loading was much lower than the strength of the rock.

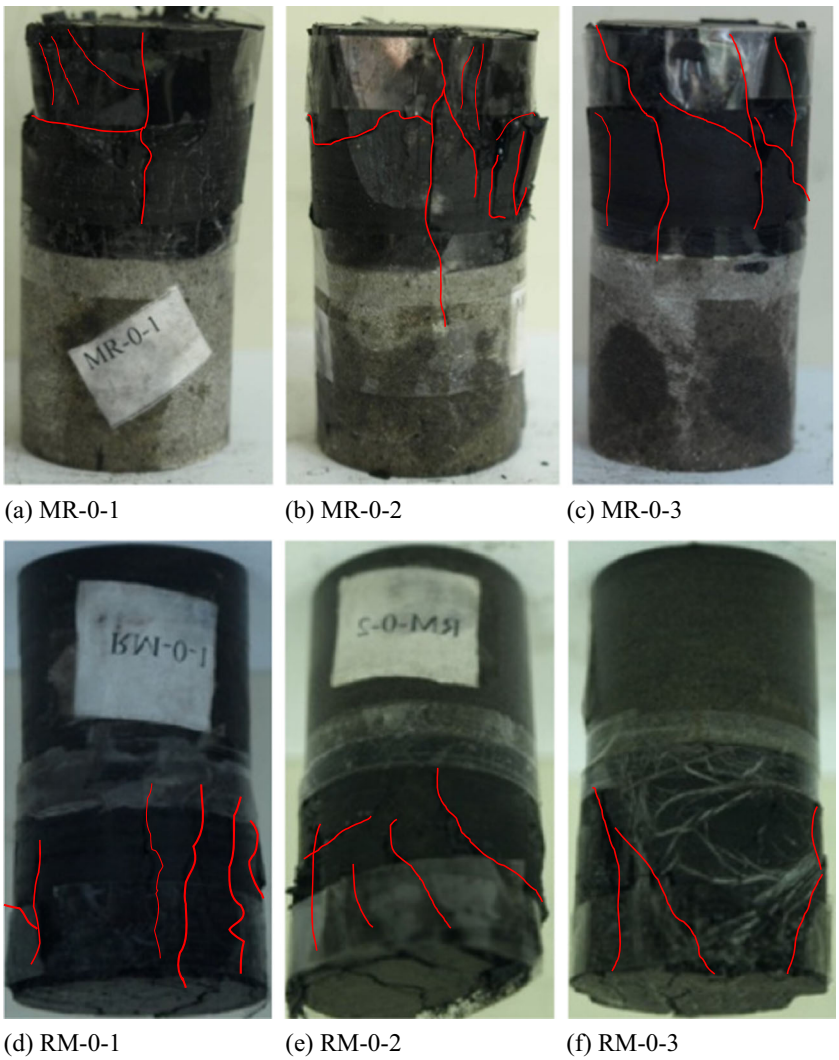

(a) MR-0-1 (b) MR-0-2 (c) MR-0-3

(d) RM-0-1 (e) RM-0-2 (f) RM-0-3

Fig. 8 Typical fracture geometries of the coal–rock combination specimens under uniaxial compression

The radial deformation of the rock was very small, whereas the radial deformation of the coal was much larger. Under uniaxial compression, the failure of the coal–rock combination specimens was accompanied by the irregular longitudinal splitting of the coal. As shown in Fig. 8, many axial splitting cracks appeared in the coal, indicating a tensile splitting mode in the coal. Also, a couple of shear cracks were observed. Moreover, the cracks ended at the interface between the coal and rock. Only one crack penetrated the entire coal part and extended into the rock for a certain distance (Fig. 8b). One possible explanation for this phenomenon is the large dynamic fracture energy of the cracking that resulted in the fracture extending into the rock until the energy was consumed.

It is worth noting that cracks are able to propagate from the soft material to the hard material when the dynamic crack propagation speed exceeds a critical value (Freund 1990; Buehler et al. 2003). The dynamic fracture in composite geomaterials deserves further investigation.

X-ray CT observation

After the uniaxial compression failure, the specimens were analysed using an X-ray micro-CT scanning system. For the horizontal cross-section, the CT images were captured from the bottom to the top at 3-mm intervals. Thus, a total of 21 images of horizontal cross-sections were obtained in the CT testing of the specimens. In addition, the vertical cross-section was also scanned. The CT images can be used to observe the macrostructure of the coal and rock. We selected the vertical cross-sectional CT images of the specimens at heights of 12, 21, 30, 39, 48, and 57 mm, as shown in Fig. 9, to explore the internal damage mechanism.

Figure 10 shows the vertical and horizontal cross-sections at different heights of the coal–rock combination specimens after uniaxial compression failure. It is observed that the CT images approximate the locations of the cracks shown in Fig. 8, which demonstrates that X-ray micro-CT scanning is suitable for exploring the internal damage in geomaterials.

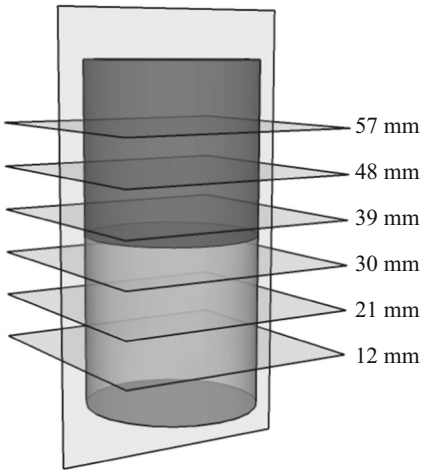

Fig. 9 Illustrations of the directions of X-ray computed tomography (CT) scanning and selected cross-section scans

The CT observations indicate that many axial cracks occurred in the coal portion and the distribution of the cracks was very complex, which resulted from the crack propagation and coalescence inside the specimen with the increase in the deformation. In contrast, no macroscopic fractures were observed in the rock portion in most of the specimens. Only one large splitting crack cut through the rock portion of specimen MR-0-2 (Fig. 10b) and a small crack was observed at the periphery of the interface between the rock and coal for specimens MR-0-3 (Fig. 10c) and RM-0-1 (Fig. 10d).

It can be seen that the extent of the internal damage due to the fractures in the coal portion in the coal–rock combination specimens after uniaxial compression failure is lower near the interface between the rock and coal and greater towards the end. This observation suggests that the cracks initiated from the interface of the coal–rock and then propagated towards the end of the coal portion.

Spatial distribution of AEs

An AE event corresponds to a crack in the specimen during the loading process. The spatial distribution of the AEs provides insights into the characteristics of the spatial distribution of the microcracks inside the specimen. The development of the microcracks of the coal–rock combined body was analysed based on the three-dimensional distribution of the AEs to provide an explanation for the macroscopic mechanical behaviour.

The spatial distributions of the AEs at different stress-level intervals in the MR and RM specimens under uniaxial compression were obtained and the examples of MR-0-1 and RM-0-3 are shown in Fig. 11. The number of AE events was extremely high during the early loading stage and then gradually decreased with increasing stress levels. In other words, a large number of microcracks occurred during the early stage of loading and very few microcracks or AE events occurred after the peak stress.

The AE events occurred throughout the loading process. The spatial distribution of the AEs was highly concentrated near the interface between the coal and rock and a conspicuous nucleation region was observed. Specifically, the AE activities occurring in the coal portion accounted for approximately 80% of the total number of AE events in the entire specimen. Because the coal has lower strength than the rock, cracking occurred more easily in the coal portion than in the rock portion under relatively low-stress conditions. The induced microcracks occurred mainly in the coal portion and it was the cracks parallel to the loading direction

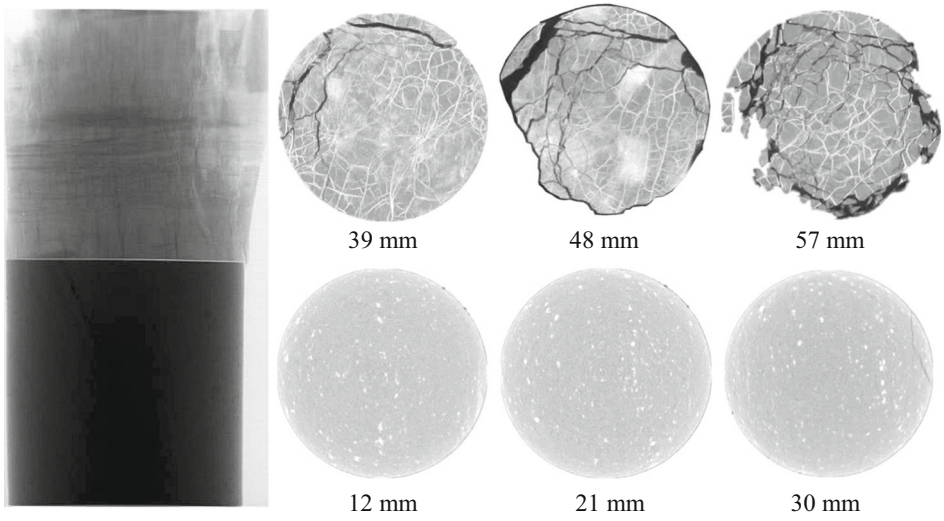

(a) MR-0-1

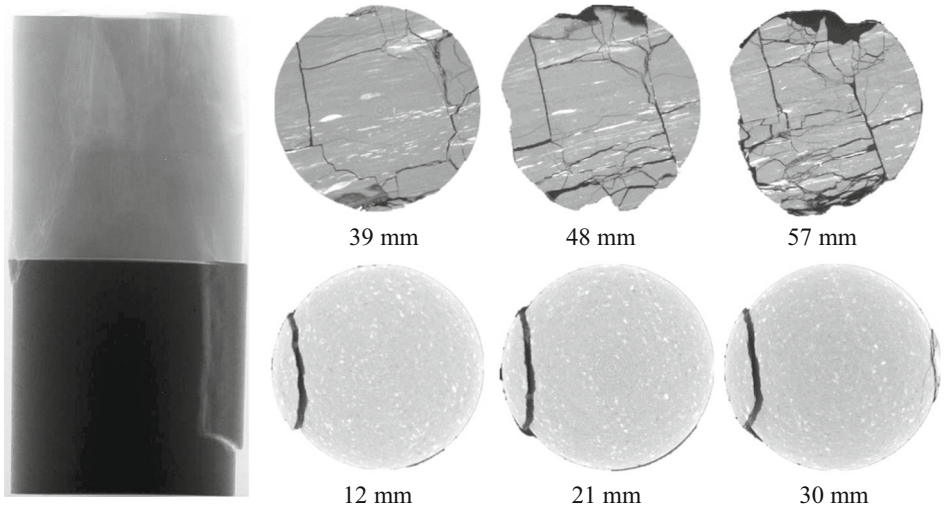

(b) MR-0-2

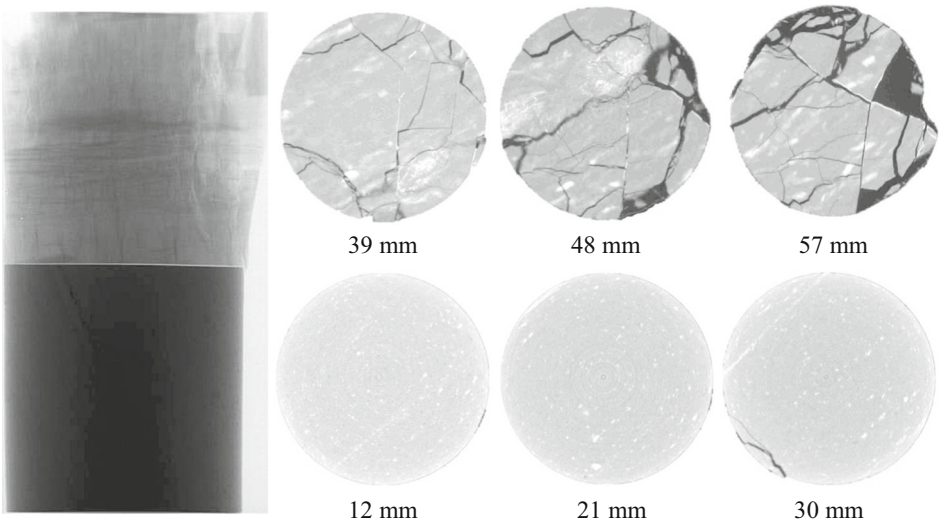

(c) MR-0-3

Fig. 10 CT images of the coal–rock combination specimens after axial compression

Fig. 10 (continued)

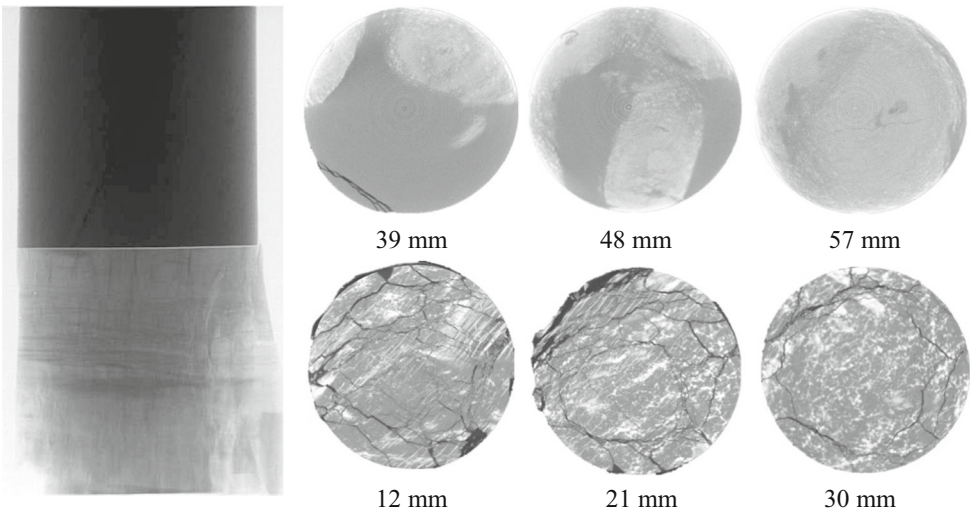

(d) RM-0-1

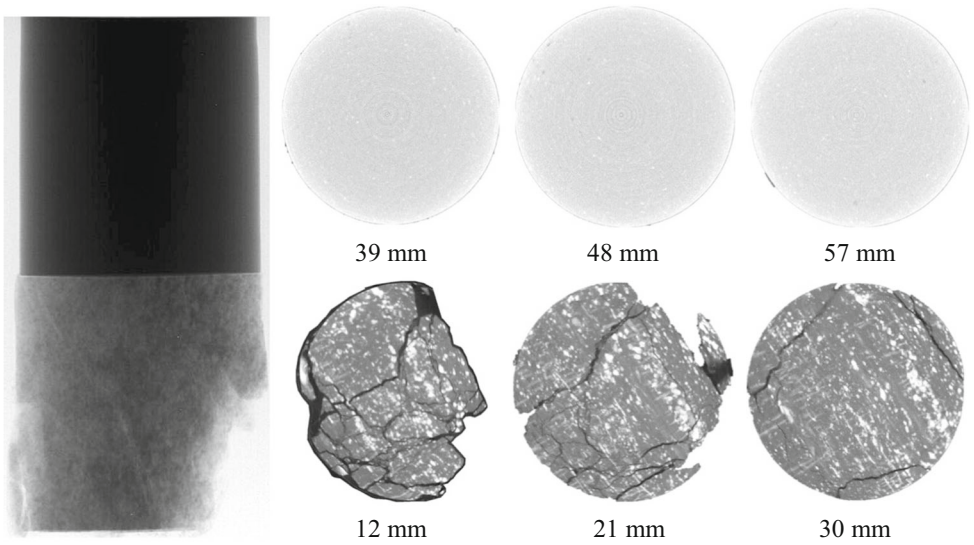

(e) RM-0-2

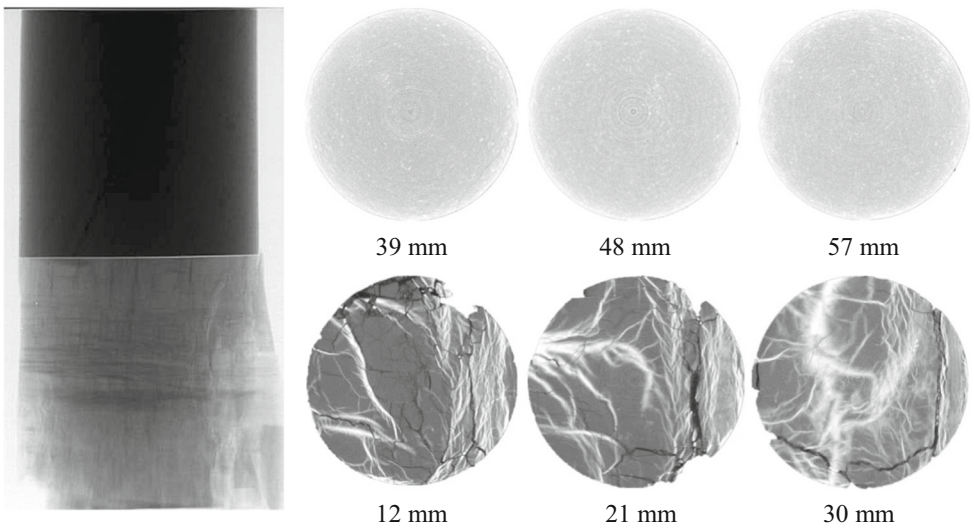

(f) RM-0-3

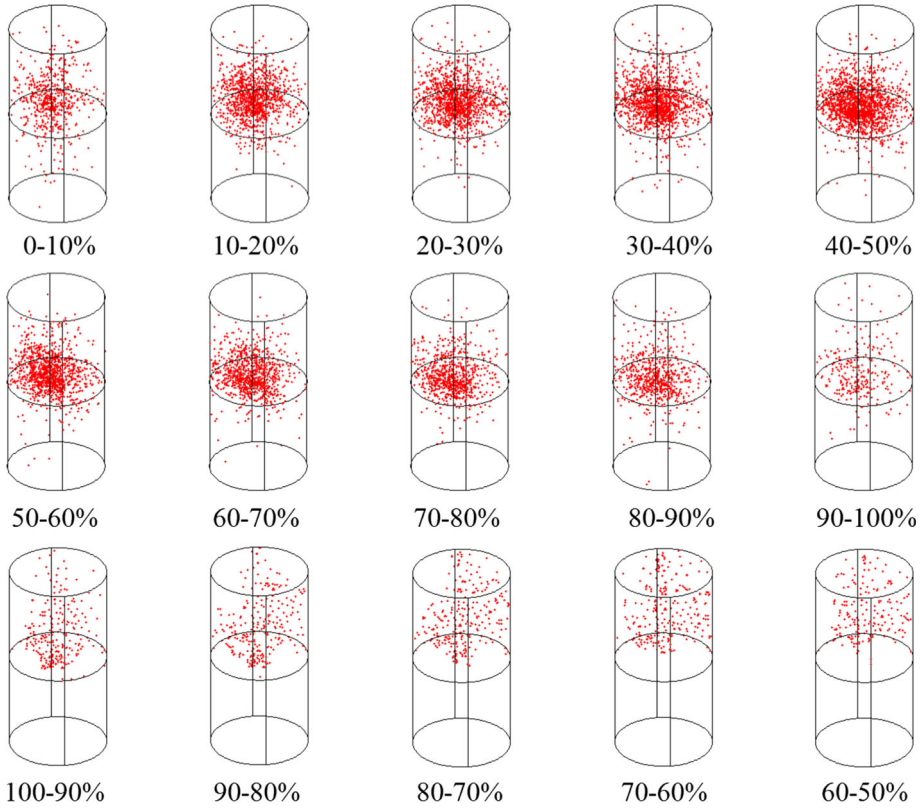

(a) MR-0-1

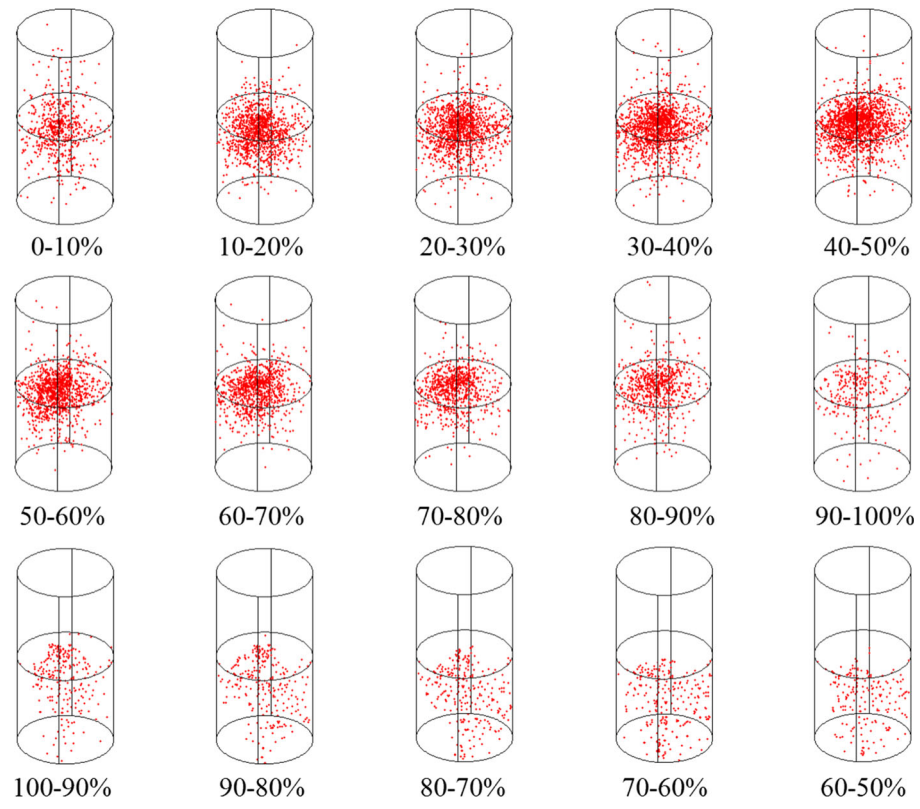

(b) RM-0-3

Fig. 11 Spatial distributions of the acoustic emissions (AEs) at different stress-level intervals in the coal–rock combined body

that resulted in the failure of the specimen in an axial splitting failure mode.

In the coal portion, microcracks were produced continuously and extended and interconnected slowly and in an orderly manner throughout the coal. Several major cracks rapidly extended and interconnected near the peak stress as the bearing capacity of the coal rapidly decreased.

It was observed that the cracks were first initiated at the interface of the coal–rock combined body and then propagated towards the weak region of the specimen. This is attributed to the different mechanical properties of the rock and coal. A complex stress state developed near the interface, including areas of stress concentration. Furthermore, due to the composite material properties of the coal–rock combined body, a more complex mechanical response than in either coal or rock bodies was observed with regard to the deformation and fracture of the component materials. The complex relationship of the stress and strain results in the interface becoming the most likely zone where cracks may first initiate and propagate (Li et al. 2009, 2014).

Numerical analysis

For a better understanding of the failure mechanism of the coal–rock combined body, the uniaxial compression tests were modelled using the three-dimensional distinct element code (3DEC). Because of the symmetry between the RM and MR specimens, a numerical model was developed for the MR specimen. The model of the coal and rock specimen had a diameter of 35 mm and a height of 35 mm, which is the same as the experimental specimens. A cohesionless connection between the coal and the rock was simulated in this case. The material properties of the rock and coal were defined based on previous experimental investigations, as shown in Table 2. Both materials were described according to the Mohr–Coulomb strength criterion. A constant displacement rate of 0.06 mm/min was applied to the upper surface of the specimen to control the failure process, whereas the lower surface was fixed.

The simulated stress–strain curves and failure patterns of the model MR specimen are shown in Fig. 12. The specimen failure was accompanied by a longitudinal splitting of the coal portion, whereas no damage and displacement occurred in the rock. These results were in general agreement with the experimental observations.

Constitutive modelling of the coal–rock combined body

Since neither rock nor coal is a perfectly elastic medium, the materials tend to retain a portion of the total deformation caused by the loading process, such as plastic deformation. Plastic deformation is due to the closing or sliding of the microcracks. Some research indicates that the rock mass also exhibits nonlinear characteristics during the elastic phase (Brown et al. 1989; Nawrocki et al. 1998; Lionço and Assis 2000; Zuo et al. 2008, 2009, 2014, 2015; Singh et al. 2015). In this section, a new nonlinear constitutive relationship is proposed.

Formulation of the constitutive model

The constitutive model to describe the stress–strain relationship of the coal–rock combined body was formulated based on the experimental data and the concept of natural (or true) volumetric strain (Freed 1995).

Figure 13 schematically shows the deformation process of the coal–rock combined body under an external load F and based on the failure mode observed in this study. Assume that a uniformly distributed force is exerted on the ends of the coal–rock combined body subject to elastic deformation. Hooke's law can be applied to the rock and coal portions and is described by Eqs. (1) and (2), respectively:

$$d\sigma_R = m_R E_R d\varepsilon_R \tag{1}$$

$$d\sigma_C = m_C E_C d\varepsilon_C \tag{2}$$

where σ_R and σ_C are the axial stresses of the rock and coal portions, respectively; E_R and E_C are the elastic modulus of the rock and coal portions, respectively; ε_R and ε_C are the axial strains of the rock and coal portions, respectively; and m_R and m_C are the correction coefficients of the elastic modulus of the rock and coal portions, respectively. In this case, only the constitutive model for the uniaxial compression is discussed.

Unlike purely solid materials that have a constant elastic modulus, rock and coal are geomaterials and have many pores

Table 2 Physical and mechanical parameters of the coal–rock combined body

Materials and properties	Elastic modulus (Gpa)	Poisson's ratio	Cohesion (MPa)	Internal friction angle (°)	Dilatancy angle (°)
Coal	3	0.33	6.74	20.82	18.5
Rock	30	0.3	26.32	25.60	23.0

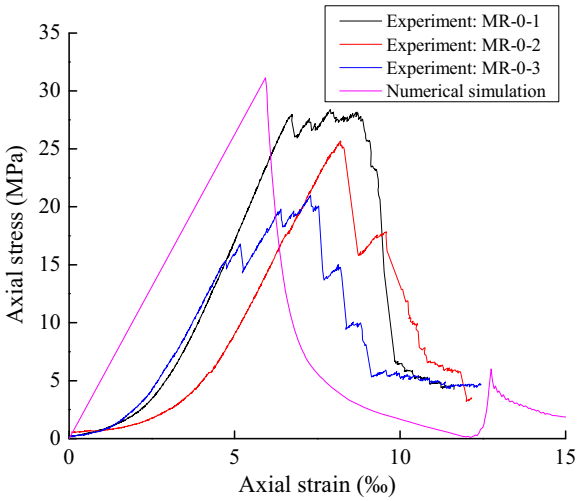

(a) Simulated and experimental stress-strain curves

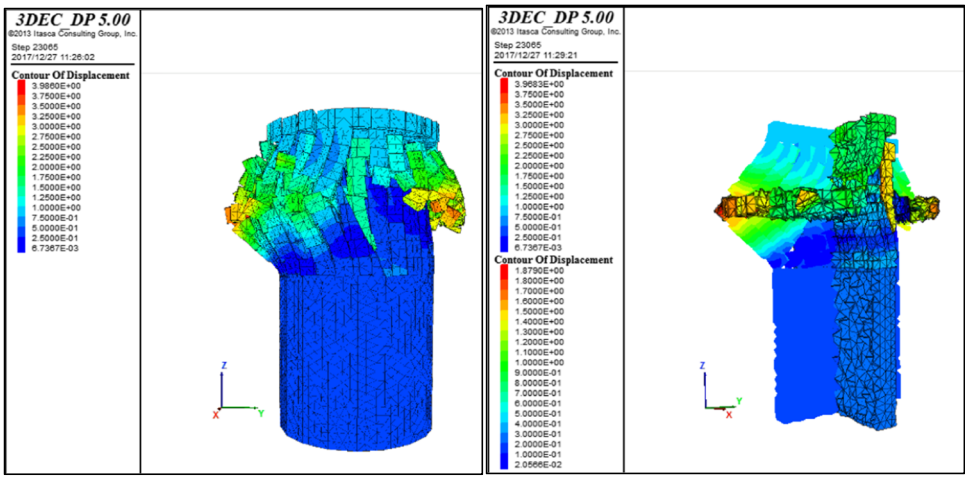

(b) Contours of displacement

(c) Profile of displacement

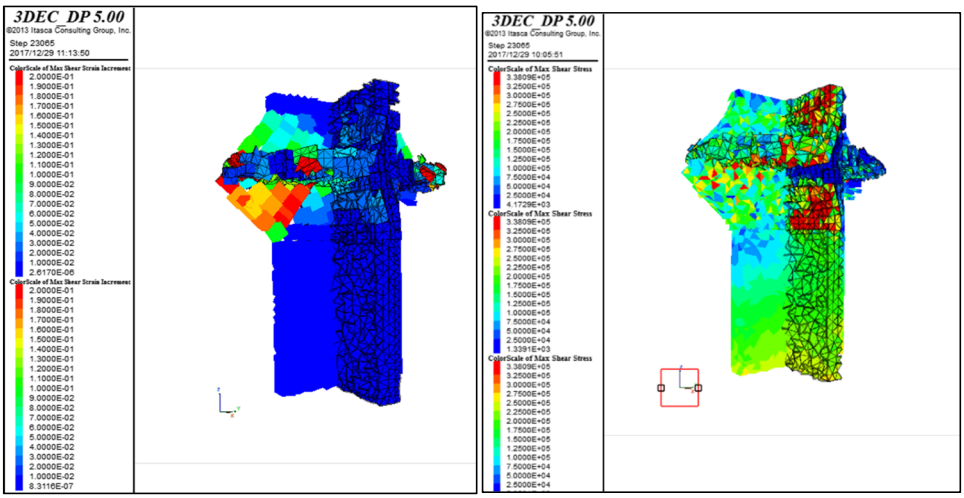

(d) Contours of maximum shear strain

(e) Contours of maximum shear stress

Fig. 12 Simulated stress–strain curves and failure patterns of the model MR specimen under uniaxial compression

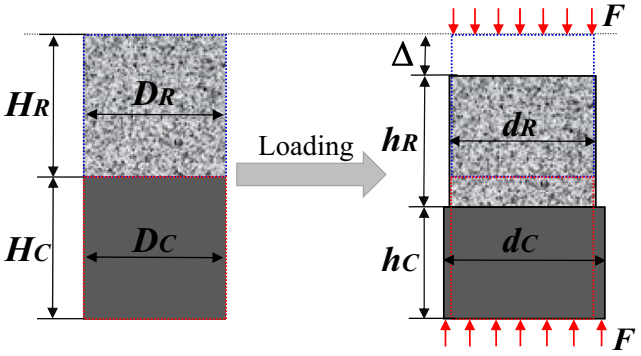

Fig. 13 Illustration of the deformation process of the coal–rock combined body under the external load F. H_R and H_C are the heights of the rock and coal at the initial state, respectively; D_R and D_C are the diameters of the rock and coal at the initial state, respectively. The subscripts R and C denote rock and coal, respectively. h_R and h_C are the heights of the rock and coal under loading F, respectively; d_R and d_C are the diameters of the rock and coal under loading F, respectively; Δ is the displacement of the combined body

and fractures of irregular sizes and shapes that result in a heterogeneous and anisotropic material. Thus, the elastic modulus of the rock E_R and coal E_C obtained from the experimental tests is not constant throughout the rock or coal body. A discreteness of the elastic modulus exists; therefore, the correction coefficients m_R and m_C for the elastic modulus are used in Eqs. (1) and (2), respectively. Since the coal–rock combined body represents a combined system, the axial force applied to the rock should be equal to that applied to the coal. Therefore, we have:

$$dF = S_R d\sigma_R = S_C d\sigma_C \tag{3}$$

where S_R and S_C are the cross-sectional areas of the rock and coal portions, respectively, and F is the axial loading.

The cross-sectional areas of the rock (S_R) and coal (S_C) portions are:

$$S_R = \pi {D_R}^2/4 \tag{4}$$

$$S_C = \pi {D_C}^2/4 \tag{5}$$

Due to the different physical and mechanical characteristics of the rock and coal, these materials can be regarded as the hard and soft parts of the coal–rock combined body. The external loading F deforms both the coal and rock. The heights of the rock and coal decrease with the increase in the external loads, whereas the diameters increase. The radial deformation of the rock is relatively small compared to that of the coal. Hence, based on Hooke's law, the strain of the rock ε_R is defined as (Jaeger et al. 2007):

$$d\varepsilon_R = -\frac{dh_R}{H_R} \tag{6}$$

where H_R is the initial length of the rock portion in an unstressed state and h_R is the current length of the rock body in a stress state. This strain calculated by Eq. (6) is termed the engineering strain (Jaeger et al. 2007). The engineering strain is used exclusively because the elastic strain is generally small.

However, coal is inherently heterogeneous because it is composed of a solid phase, pores and fractures with a variety of geometric shapes and sizes. The elastic strain of the coal is relatively small with regard to changes in the stress that are of practical interest, but the elastic strain of the pores and fractures is relatively large. The pores and fractures in the coal can be subject to significant deformation and can even close completely under a certain range of stress encountered in practical applications.

In this case, a large error would result if the engineering strain method was used. Many researchers have argued that the natural strain should be used for the accurate description of material deformation (Freed 1995), including the deformation of geomaterials (Liu et al. 2009, 2011; Wood 1973). The natural strain of coal $d\varepsilon_C$ is defined as (Freed 1995):

$$d\varepsilon_C = -\frac{dh_C}{h_C} \tag{7}$$

where h_C is the length of the coal body in the current stress state.

The integration of Eqs. (1), (2), (6) and (7) yields the stress of coal and rock:

$$\begin{cases} \sigma_R = -\dfrac{m_R E_R}{H_R} h_R + C_R \\ \sigma_C = -m_C E_C \ln h_C + C_C \end{cases} \tag{8}$$

where C_R and C_C are integral constants for the rock and coal, respectively.

Subsequently, using the initial conditions of $h_R = H_R$ and $h_C = H_C$ when $\sigma = 0$, the integral constants can be obtained:

$$\begin{cases} C_R = m_R E_R \\ C_C = m_C E_C \ln H_C \end{cases} \tag{9}$$

Based on Eqs. (8) and (9), the displacement of the rock and coal can be obtained as:

$$\begin{cases} \Delta_R = h_R - H_R = -H_R \dfrac{\sigma_R}{m_R E_R} \\ \Delta_C = h_C - H_C = H_C \left[\exp\left(-\dfrac{\sigma_C}{m_C E_C} \right) - 1 \right] \end{cases} \tag{10}$$

where Δ_R and Δ_C are the changes in the lengths of the rock and coal under stress, respectively.

It is evident from Eq. (10) that the deformation of the rock is linear and the deformation of the coal is nonlinear. The deformation of the coal is nonlinear because of the heterogeneity of the pore geometry and the non-uniform pore size

distribution in the coal and at the interface between the coal and rock. Considering the compression of the cracks and pores and the interface during the compaction stage, a coefficient k_C is introduced.

Thus, the total displacement Δ of the coal–rock combined body under uniaxial compression can be obtained as:

$$-\Delta = H_R\frac{\sigma_R}{m_R E_R} + k_C H_C\left[1-\exp\left(-\frac{\sigma_C}{m_C E_C}\right)\right] \quad (11)$$

By combining Eqs. (3) and (11), the load–displacement relationship of the coal–rock combined body is given as:

$$-\Delta = H_R\frac{F}{S_R m_R E_R} + k_C H_C\left[1-\exp\left(-\frac{F}{S_C m_C E_C}\right)\right] \quad (12)$$

By substituting Eqs. (4) and (5) into the cross-sectional areas of the rock (S_R) and coal (S_C) portions in Eq. (12), we obtain:

$$-\Delta = H_R\frac{4F}{\pi D_R^2 m_R E_R} + k_C H_C\left[1-\exp\left(-\frac{4F}{\pi D_C^2 m_C E_C}\right)\right] \quad (13)$$

Equation (13) is the proposed load–displacement relationship for the coal–rock combined body. We should emphasise that our theory is a macroscopic-scale approximation that uses the natural strain-based Hooke's law to describe the nonlinear deformation behaviour of a coal–rock combined body subject to large deformations.

Verification of the model

The uniaxial compression tests performed on the coal–rock combined body exhibited significant nonlinear elastic deformation prior to peak stress. The characterisation of the nonlinear elastic deformation is more complex for the coal–rock combined body. Here, a general methodology for the determination of the model parameters for the stress–strain characteristics is proposed and briefly outlined.

The equations involve ten parameters that can be determined directly from the interpretation of the uniaxial tests. H_R, D_R, H_C and D_C were directly measured prior to the test (Table 1). F was recorded automatically and continuously by the test system. E_R and E_C were determined from the linear part of the stress–strain curves obtained in the uniaxial compression tests and the average values ($E_R = 31.57$ GPa and $E_C = 3.75$ GPa) were obtained based on various tests (Zuo et al. 2011a, b). m_R, m_C and k_C were identified by applying other parameters to Eq. (12), and their values determined are listed in Table 3.

The uniaxial compression tests were simulated using the proposed model and the obtained parameters. Figure 14 shows comparisons of the numerical simulations and experimental data. The proposed model correctly described the pre-peak behaviours of the coal–rock combined body but failed to reproduce the softening phenomenon during the post-peak regime. The derivation of a constitutive model able to simultaneously describe the pre- and postpeak behaviours of coal–rock combined bodies will be considered in a follow-up study.

Table 3 Values of m_R, m_C and k_C

Sample no.	m_R	m_C	k_C
MR-0-1	0.112	0.00460	0.000756
MR-0-2	0.082	0.00692	0.000721
MR-0-3	0.050	0.00244	0.000227
RM-0-1	0.160	0.00233	0.000354
RM-0-2	0.091	0.00349	0.000586
RM-0-3	0.080	0.00108	0.000542

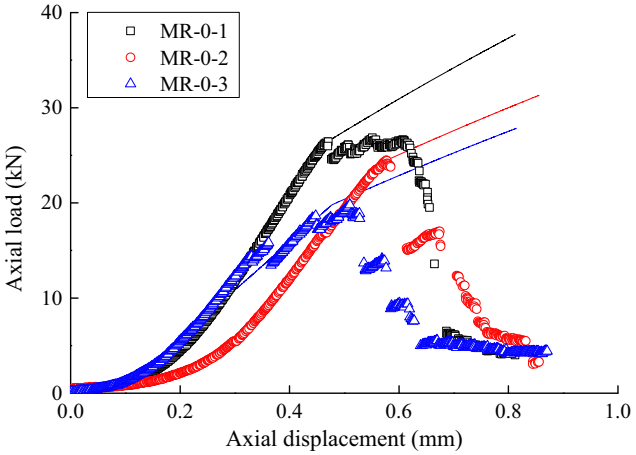

(a) MR

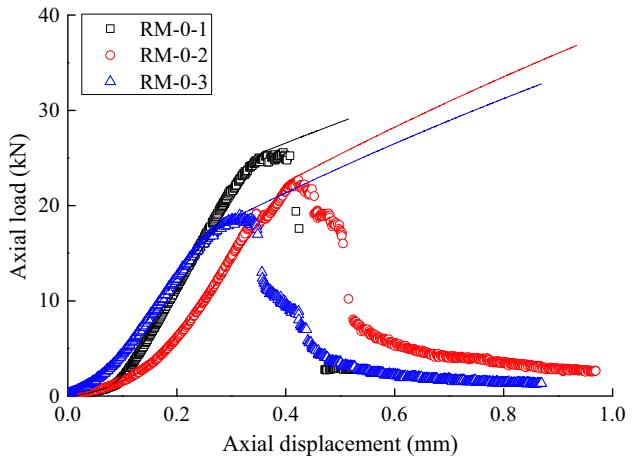

(b) MR

Fig. 14 Comparison of the experimental and simulated results of the uniaxial compression tests (the solid line represents the numerical results)

Implications for underground mining risks

The surrounding rocks around coal roadways are composite structures composed of weakly cemented soft coal and hard rock, and the roadway stability is closely related to the overall mechanical behaviour of the combined body. Based on the analysis of the uniaxial compression experiments and numerical simulations, it is concluded that the fracture and deformation characteristics are mainly influenced by the coal seam.

During deep mining, the stress is redistributed and the maximum and minimum stresses occur near the roadway, which increases the fracture risk of the coal seam. Due to the differences in the stress distribution in the rock and coal, when the coal enters the strain-hardening stage, the rock mass is usually in the elastic deformation stage and the burst risk of the coal is high. Cracking in the coal body under excavation stress induces instability and leads to bursts in the coal. If the crack propagates at a sufficiently high speed and has enough energy to damage the roof rock, then coal and rock bursts may occur. This is the main mechanism whereby coal bumps or coal and rock bursts occur after excavation unloading. This study has deepened our understanding of the mechanisms of coal–rock compound dynamic disasters and provides theoretical bases for their predictions during coal mining.

Conclusions and recommendations

To study the deformation failure characteristics of coal–rock combined body in a systematic manner, a series of uniaxial tests were performed on specimens. Based on an experimental investigation, a constitutive model for elastic deformation is proposed. The main concluding remarks are as follows:

(1) The uniaxial compression curve of the coal–rock combined body exhibited six distinct phases and typical brittle mechanical behaviour.
(2) The mechanical properties and deformation failure characteristics of the coal–rock combined body were influenced mainly by the coal. The mechanical properties of the coal dominated the properties of the combined bodies. The uniaxial compressive strength (UCS) and elastic modulus of the coal–rock combined body were slightly larger than those of the coal and much smaller than those of the rock. The failure of the coal–rock combined body was dominated by axial splitting tensile cracks in the coal, following a tensile splitting mode. The interface was the most likely zone where cracks first initiated and propagated.
(3) A constitutive model was proposed to characterise the coal–rock combined bodies using the concept of natural strain. The proposed model describes the pre-peak behaviour quite well. The derivation of a general model describing the overall mechanical behaviour of coal–rock combined bodies will be considered in a follow-up study.
(4) The existence of the weak coal changes the overall failure mechanism and strength in a coal–rock combined body, thereby reducing the overall stability of a coal roadway. Furthermore, it should be noted that the deformation and failure of the coal–rock combined body have an important influence on the design and excavation of coal roadways in large cutting height coalfaces.

This preliminary study is intended to deepen our understanding of the mechanisms of coal and rock dynamic disasters and provide theoretical bases for their predictions. However, this study does not consider the stress release and size effects, although they may be of interest in a follow-up study to validate the results of this study. Unloading and multi-scale tests will be conducted, allowing the stress release and size effects to be investigated precisely in the near future.

Acknowledgements The authors gratefully acknowledge the support from the National Natural Science Foundation of China (51622404 and 11572343), Yueqi Distinguished Scholar of CUMTB, the State Key Research Development Program of China (2016YFC0801404), National Program for Support of Top-notch Young Professionals and China Postdoctoral Science Foundation (2017 M620048 and 2018 T110103).

References

Brown ET, Bray JW, Santarelli FJ (1989) Influence of stress-dependent elastic moduli on stresses and strains around axisymmetric boreholes. Rock Mech Rock Eng 22(3):189–203

Buehler MJ, Abraham FF, Gao HJ (2003) Hyperelasticity governs dynamic fracture at a critical length scale. Nature 426(6963):141–146

Cao A, Dou L, Cai W, Gong S, Liu S, Jing G (2015) Case study of seismic hazard assessment in underground coal mining using passive tomography. Int J Rock Mech Min Sci 78:1–9

Freed AD (1995) Natural strain. J Eng Mater Technol 117(4):379–385

Freund LB (1990) Dynamic fracture mechanics. Cambridge University Press, Cambridge

Gao FQ, Stead D, Kang HP (2014) Numerical investigation of the scale effect and anisotropy in the strength and deformability of coal. Int J Coal Geol 136:25–37

Gao F, Stead D, Kang H (2015) Numerical simulation of squeezing failure in a coal mine roadway due to mining-induced stresses. Rock Mech Rock Eng 48(4):1635–1645

Ghasemi E, Ataei M, Shahriar K (2014) An intelligent approach to predict pillar sizing in designing room and pillar coal mines. Int J Rock Mech Min Sci 65:86–95

Jaeger JC, Cook NGW, Zimmerman RW (2007) Fundamentals of rock mechanics, 4th edn. Blackwell, Oxford

Kang HP, Lou JF, Gao FQ, Yang JH, Li JZ (2018) A physical and numerical investigation of sudden massive roof collapse during longwall coal retreat mining. Int J Coal Geol 188:25–36

Konicek P, Soucek K, Stas L, Singh R (2013) Long-hole destress blasting for rockburst control during deep underground coal mining. Int J Rock Mech Min Sci 61:141–153

Kwinta A (2012) Prediction of strain in a shaft caused by underground mining. Int J Rock Mech Min Sci 55:28–32

Li YP, Yang CH, Daemen JJK, Yin XY, Chen F (2009) A new Cosserat-like constitutive model for bedded salt rocks. Int J Numer Anal Meth Geomech 33(15):1691–1720

Li LC, Yang TH, Liang ZZ, Zhu WC, Tang CN (2011) Numerical investigation of groundwater outbursts near faults in underground coal mines. Int J Coal Geol 85(3–4):276–288

Li YP, Liu W, Yang CH, Daemen JJK (2014) Experimental investigation of mechanical behavior of bedded rock salt containing inclined interlayer. Int J Rock Mech Min Sci 69:39–49

Lionço A, Assis A (2000) Behaviour of deep shafts in rock considering nonlinear elastic models. Tunn Undergr Sp Tech 15(4):445–451

Liu HH, Rutqvist J, Berryman JG (2009) On the relationship between stress and elastic strain for porous and fractured rock. Int J Rock Mech Min Sci 46(2):289–296

Liu HH, Rutqvist J, Birkholzer JT (2011) Constitutive relationships for elastic deformation of clay rock: data analysis. Rock Mech Rock Eng 44(4):463–468

Liu J, Wang EY, Song DZ, Wang SH, Niu Y (2015) Effect of rock strength on failure mode and mechanical behavior of composite samples. Arab J Geosci 8(7):4527–4539

Meng Z, Shi X, Li G (2016) Deformation, failure and permeability of coal-bearing strata during longwall mining. Eng Geol 208:69–80

Nawrocki PA, Dusseault MB, Bratli RK, Xu G (1998) Assessment of some semi-analytical models for non-linear modelling of borehole stresses. Int J Rock Mech Min Sci 35(4–5):522

Paterson MS, Wong TF (2005) Experimental rock deformation—the brittle field, 2nd edn. Springer, New York

Petukhov IM, Linkov AM (1979) The theory of post-failure deformations and the problem of stability in rock mechanics. Int J Rock Mech Min Sci Geomech Abstr 16:57–76

Qian QH (2004) The current development of nonlinear rock mechanics: the mechanics problems of deep rock mass. In: Chinese Society of Rock Mechanics and Engineering (ed) Proceedings of the 8th rock mechanics and engineering conference. Science Press, Beijing, pp 10–17 (in Chinese)

Singh M, Samadhiya NK, Kumar A, Kumar V, Singh B (2015) A nonlinear criterion for triaxial strength of inherently anisotropic rocks. Rock Mech Rock Eng 48(4):1387–1405

Tsang CF, Bernier F, Davies C (2005) Geohydromechanical processes in the excavation damaged zone in crystalline rock, rock salt, and indurated and plastic clays—in the context of radioactive waste disposal. Int J Rock Mech Min Sci 42:109–125

Ulusay R, Hudson JA (2007) The complete ISRM suggested methods for rock characterization, testing and monitoring: 1974–2006. Commission on Testing Methods, International Society of Rock Mechanics

Wang H, Jiang Y, Zhao Y, Zhu J, Liu S (2013) Numerical investigation of the dynamic mechanical state of a coal pillar during longwall mining panel extraction. Rock Mech Rock Eng 46(5):1211–1221

Wang T, Jiang YD, Zhan SJ, Wang C (2014) Frictional sliding tests on combined coal–rock samples. J Rock Mech Geotech Eng 6(3):280–286

Wang G, Wu M, Wang R, Xu H, Song X (2017a) Height of the mining-induced fractured zone above a coal face. Eng Geol 216:140–152

Wang K, Du F, Zhang X, Wang L, Xin C (2017b) Mechanical properties and permeability evolution in gas-bearing coal–rock combination body under triaxial conditions. Environ Earth Sci 76(24):815

Wood DS (1973) Patterns and magnitudes of natural strain in rocks. Phil Trans R Soc Lond A 274(1239):373–382

Xie HP, Zhao XP, Liu JF, Zhang R, Xue DJ (2012a) Influence of different mining layouts on the mechanical properties of coal. Int J Min Sci Technol 22:749–755

Xie HP, Zhou HW, Xue DJ, Wang HW, Zhang R, Gao F (2012b) Research and consideration on deep coal mining and critical mining depth. J China Coal Soc 37(4):535–542 (in Chinese)

Yang W, Lin BQ, Zhai C, Li XZ, An S (2012) How in situ stresses and the driving cycle footage affect the gas outburst risk of driving coal mine roadway. Tunn Undergr Sp Technol 31:139–148

Yang W, Wang H, Lin BQ, Wang YK, Mao XB, Zhang JG, Lyu YC, Wang M (2018) Outburst mechanism of tunnelling through coal seams and the safety strategy by using "strong–weak" coupling circle-layers. Tunn Undergr Sp Technol 74:107–118

Zhang Z, Zhang R, Xie H, Liu J, Were P (2015) Differences in the acoustic emission characteristics of rock salt compared with granite and marble during the damage evolution process. Environ Earth Sci 73(11):6987–6999

Zhang Y, Chen Y, Yu R, Hu L, Irfan M (2017) Effect of loading rate on the felicity effect of three rock types. Rock Mech Rock Eng 50(6):1673–1681

Zhao ZH, Wang WM, Wang LH, Dai CQ (2015) Compression–shear strength criterion of coal–rock combination model considering interface effect. Tunn Undergr Sp Technol 47:193–199

Zhu SY, Jiang ZQ, Zhou KJ, Peng GQ, Yang CW (2014) The characteristics of deformation and failure of coal seam floor due to mining in Xinmi coal field in China. B Eng Geol Environ 73(4):1151–1163

Zuo JP, Li HT, Xie HP, Ju Y, Peng SP (2008) A nonlinear strength criterion for rock-like materials based on fracture mechanics. Int J Rock Mech Min Sci 45(4):594–599

Zuo JP, Peng SP, Li YJ, Chen ZH, Xie HP (2009) Investigation of karst collapse based on 3-D seismic technique and DDA method at Xieqiao coal mine, China. Int J Coal Geol 78(4):276–287

Zuo JP, Pei JL, Liu JF, Peng R, Li YC (2011a) Investigation on acoustic emission behavior and its time–space evolution mechanism in failure process of coal–rock combined body. Chin J Rock Mech Eng 30(8):1564–1570 (in Chinese)

Zuo JP, Xie HP, Wu AM, Liu J (2011b) Investigation on failure mechanisms and mechanical behaviors of deep coal–rock single body and combined body. Chin J Rock Mech Eng 30(1):84–92 (in Chinese)

Zuo JP, Xie HP, Dai F, Ju Y (2014) Three-point bending test investigation of the fracture behavior of siltstone after thermal treatment. Int J Rock Mech Min Sci 70:133–143

Zuo JP, Liu HH, Li HT (2015) A theoretical derivation of the Hoek–Brown failure criterion for rock materials. J Rock Mech Geotech Eng 7(4):361–366

Zuo JP, Chen Y, Zhang JW, Wang JT, Sun YJ, Jiang GH (2016) Failure behavior and strength characteristics of coal–rock combined body under different confining pressures. J China Coal Soc 41:2706–2713 (in Chinese)